Distinguishing Impacts of Molecular Weight Fractionated Suwannee River Natural Organic Matter on the Aggregation of Fullerene Nanoparticles in Mono- and Di-valent Electrolyte Solutions

Mo-hai Shen[†], Yong-guang Yin[†], Andy Booth[‡], Jing-fu Liu[*,†]

[†]State Key Laboratory of Environmental Chemistry and Ecotoxicology, Research Center for Eco-Environmental Sciences, Chinese Academy of Sciences, Beijing 100085, China

[‡]SINTEF Materials and Chemistry, Trondheim, NO-7465, Norway

* Corresponding Author

Tel.: +86-10-62849192; Fax: +86-10-62849192;

E-mail: jfliu@rcees.ac.cn.

ABSTRACT

Elucidating the toxicity and risks of Fullerene nanoparticles (nC_{60}) calls for intensive studies on its environmental fate and behavior, which highly depends on fundamental processes like the aggregation of nC_{60} in the aqueous environment. This further relies on understanding the impacts of specific fractions of natural organic matter (NOM), which is ubiquitous and heterogeneous in physical and chemical properties. In this study, we comprehensively investigated monovalent (Na^+) and divalent (Ca^{2+} and Mg^{2+}) electrolyte-induced aggregations of nC_{60} in the presence of molecular weight fractionations of Suwannee River NOM (M_f-SRNOMs) prepared by ultrafiltration separation. Possible molecular weight (MW), structure and functional group dependent effects of M_f-SRNOMs on the initial aggregation kinetics of nC_{60} were quantitatively assessed. We observed that, the aromatic structures were abundant in high M_f-SRNOMs, while carboxylic groups were more abundant in low M_f-SRNOMs. At low concentrations of both monovalent and divalent electrolytes, high MW M_f-SRNOM (1 mg L^{-1} as carbon) provided significantly enhanced dispersion stability of nC_{60} than the low ones. At high NaCl concentrations, the stability of nC_{60} was positively correlated to the MW of M_f-SRNOMs. However, due to the complexation/cation-bridging effect of Ca^{2+} (Mg^{2+}) with carboxylic groups in M_f-SRNOMs, enhanced aggregation kinetics of nC_{60} was observed in the majority of M_f-SRNOM/divalent-electrolyte solutions, especially for high MW M_f-SRNOMs (SRNOM>100 kD and SRNOM 30-100 kD). Overall, high MW M_f-SRNOMs provided significantly different influences on nC_{60} aggregation in the presence of monovalent/divalent electrolytes, compared with their low MW counterparts. Results strongly indicated that (i) the MW-dependent steric-hindrance effect of M_f-SRNOMs is primary responsible for defending nC_{60} from electrolyte induced aggregation; (ii) the differences in the abundance of aromaticity and carboxylic groups of M_f-SRNOMs result in M_f-SRNOM-dependent nC_{60} aggregation, resulting from more complex interactions between M_f-SRNOM-nC_{60}-electrolyte.

INTRODUCTION

Fullerenes (C_{60}) and carbon nanotubes (CNTs) are among the most widely used engineered nanoparticles (ENPs) in industry and consumer products.[1-3] In addition, naturally occurring C_{60} is also widely observed in natural carbonaceous materials[4] and combustion process.[5] Although it has an extremely low water solubility,[6] molecular C_{60} can form stable nanoscale aggregates (nC_{60}) in water through solvent-exchange and extended stirring.[7, 8] More importantly, natural organic matter (NOM) in aqueous environments can significantly increase the stability of dispersed nC_{60},[9] thus resulting in chronic environmental exposures to pelagic species. Despite the low toxicity of nC_{60} to aquatic organisms[10] and limited hazard through human exposure,[11] under light exposure and in the presence of O_2, nC_{60} can be highly toxic through O_2^- formation.[12] Another emerging environmental issue is the role of nC_{60} as a contaminant carrier, which influence the transport, fate and bioavailability of nC_{60}-absorbed contaminants in aqueous environments, and is strongly dependent on the physical and chemical properties of a contaminant.[13] Elucidating the toxicity and risks of nC_{60} requires more detailed studies on its environmental fate and behavior,[14-16] which is highly dependent on fundamental processes such as the aggregation of nC_{60} in the aqueous environment.

The inevitable encounter of NOM upon the released nC_{60} and other ENPs in the environment has increased the interest in their active interactions.[14, 15, 17-19] In previous studies, attempts have been made to extend the understanding of the ENP interactions with bulk[17] or specific components[19-23] of NOM, such as humic acid (HA), fulvic acid (FA) and low-molecular-weight organic acids. It was observed that nC_{60} could be stabilized in the presence of bulk or specific components of NOM by invoking steric repulsion[9, 24, 25] resulting from adsorbed NOM layers on nC_{60}. Moreover, FA was found to be less effective than HA as FA has a lower affinity with nC_{60} due to its higher charge

density and smaller aromatic backbone.[26] In addition, the occurrence of homoaggregation of HA-nC_{60}[27] could lead to the enhanced aggregation of nC_{60} in solutions exhibiting high concentrations of divalent cations compared to aggregation behavior in monovalent electrolyte solutions.[9]

NOM is a poorly defined, complex mixture of molecules with different physical structures, chemical compositions, functional group components, spectroscopic and photochemical properties,[28-33] and which can be regarded as a heterogeneous structure consisting of hydrophobic backbones and hydrophilic side chains.[25] In aqueous environments, the structure of NOM is closely related to its chemical composition and functional groups, and the molecular size, shape and aggregation state are considered as key factors influencing physicochemical reactions.[34, 35] In addition, electrolytes and pH can govern the surface charge and spectroscopic/photochemical properties of NOM in solutions.[31, 36] Furthermore, interactions such as cation-bridging between functional groups in/among NOM, leading to the neutralization of NOM surface charge, can influence the NOM structure.[35, 37-39] Therefore, it is of great interest to systematically study the effects of molecular weight (MW) distribution of NOM on ENP aggregation, both in the presence and absence of divalent electrolytes.

To date, only a single study has been reported regarding the influence of simply fractionated NOM (molecular weight >100 kD and <100 kD) on the aggregation behavior of gold nanoparticles in NaCl solutions.[40] There is currently no published data on the influence of MW distribution of NOM on the aggregation of nC_{60}, and there is a large knowledge gap about the molecular-weight-induced heterogeneity of NOM on the aggregation of nC_{60}. To the best of our knowledge, no studies have considered the influence of divalent electrolyte concentrations on the MW-dependent

homoaggregation of NOM with ENPs.

The objective of this study is to understand the effects of molecular weight fractions of NOM on the aggregation kinetics of nC_{60}. To this end, pristine Suwannee river natural organic matter (SRNOM) and isolated molecular weight fractions of SRNOM were comprehensively characterized, and their impacts on nC_{60} aggregation investigated in monovalent and divalent electrolyte solutions at varying concentrations. To our knowledge, this is the first study on the impacts of MW distribution and chemical properties' heterogeneity of NOM on the aggregation behavior of nC_{60}.

MATERIALS AND METHODS

Materials. Suwannee river natural organic matter (SRNOM, 1R101N) was obtained from the International Humic Substances Society (St. Paul，MN). C_{60} powder (purity greater than 95%) was obtained from Sigma-Aldrich (St. Louis, MO). All solutions and suspensions were prepared using 18 MΩ cm water produced with a Millipore Milli-Q Gradient system (Billerica, MA). Toluene was obtained from Fisher Scientific (Fair Lawn, NJ). Other reagents were purchased from Sinopharm Chemical Reagent Co. Ltd. (Beijing, China).

Preparation of Pristine and Molecular Weight Fractions of SRNOM. A 500 mg sample of SRNOM was dispersed in 500 mL of deionized water and stirred for 12 h in dark. The solution was then filtered through a 0.45 μm pore-size hybrid fiber membrane to remove any undissolved SRNOM. This filtered solution was referred to as pristine-SRNOM. Molecular weight-based fractionation of pristine-SRNOM was performed using ultrafiltration techniques with 15 mL centrifugal filter units from Millipore (Billerica, MA) with nominal molecular weight cut-offs (MWCO) of 100, 30, 10 and 3 kD. All filter units were pretreated by rinsing with Milli-Q water to remove residual glycerol. The fractionation of pristine-SRNOM was conducted stepwise with 30 min

113 centrifugation, at 6000-9000 rpm, for each round. Beginning with the highest MWCO, the filtrate
114 was collected and introduced into the cells with a lower MWCO for separation, and the residue was
115 carefully collected. The molecular weight fractions of SRNOM (collectively referred to as
116 M_f-SRNOMs) obtained from the separation >100 kD, 30-100 kD, 10-30 kD, 3-10 kD and lower than
117 3 kD. These were referred to as SRNOM>100, SRNOM30-100, SRNOM10-30, SRNOM3-10 and
118 SRNOM<3 respectively. All the pristine- and M_f-SRNOMs (collectively referred as SRNOMs) stock
119 solutions were stored in the dark at 4°C until used. The concentration (as carbon) of
120 pristine-SRNOM stock solution and each M_f-SRNOM was determined using a Teledyne Tekmar
121 Fusion total organic carbon (TOC) analyzer (Mason, Ohio).

122 **Spectroscopic Characterization of Pristine- and M_f-SRNOMs.** UV-vis spectrophotometric
123 analysis and fluorescence excitation-emission matrices (EEMs) of the samples were performed for
124 comprehensively characterizing pristine- and M_f-SRNOMs. Experimental details are given in the
125 Supporting Information.

126 **Preparation and Characterization of nC_{60} Suspension.** The aqueous nC_{60} suspension was
127 prepared by a modified solvent-exchange method.[19] Ninety mg C_{60} was added to 90 mL toluene,
128 extensively suspended by sonication at 600 W for 1 h, and then introduced to 900 mL
129 nitrogen-purged Milli-Q water (toluene/water=1:10 (v/v)). The mixture was subsequently shaken for
130 12 h. The toluene in the mixture was removed by nitrogen purge with sonication at 600 W for 6 h in
131 25 min cycles with 5 min intervals. The suspension was sequentially filtered using 20 μm, 2 μm and
132 0.45 μm mixed-cellulose-ester membranes. The resulting clear yellow suspension of nC_{60} was stored
133 in the dark at 4°C until use. The nC_{60} concentration in the stock suspension was 9.50 mg L^{-1}, which
134 was determined by HPLC measurement (Supporting Information). Particle size, morphology and

physicochemical properties of nC_{60} were characterized using H-7500 transmission electron microscopy (TEM, Hitachi, Japan), dynamic light scattering (DLS) and phase analysis light scattering using Malvern ZEN3600 Zetasizer Nano (Worcestershire, UK) and UV-vis spectroscopy (Supporting Information). The Z-average hydrodynamic radius of nC_{60} was routinely tested by DLS throughout the duration of the experiments.

Electrophoretic Mobility Measurement. The electrophoretic mobility (EPM) of nC_{60} in various electrolyte solution conditions was measured using a ZEN3600 Zetasizer Nano at 25 °C. The details for the EPM measurements are given in Supporting Information.

Aggregation Kinetics of nC_{60} by Time-resolved DLS. Time-resolved DLS (TR-DLS) measurements using a ZEN3600 Zetasizer Nano were conducted to investigate the aggregation of the nC_{60} suspension under various solution conditions. The detector employed a laser source of 633 nm and detection angle of 173° with each correlation function being accumulated over 10s.

The aggregation kinetics of nC_{60} was first tested in three electrolyte solutions without SRNOM. To investigate the effects of M_f-SRNOMs on nC_{60} aggregation, the pristine- or each M_f-SRNOM solution was added to the nC_{60} dispersion in disposable polystyrene cuvettes (Sarstedt, Germany). Then monovalent electrolyte (NaCl) or divalent electrolytes ($CaCl_2$ and $MgCl_2$) was added into the cuvette to initiate nC_{60} aggregation. The pH of all samples was adjusted to 7.5 with 1 mmol L^{-1} phosphate or borate buffer. For each sample, the final volume was 1 mL, with 1 mg L^{-1} nC_{60} and 1 mg L^{-1} SRNOM. The details for the TR-DLS measurements, calculation methods for attachment efficiency (α) and critical coagulation concentration (CCC) are given in Supporting Information.

RESULTS AND DISCUSSION

Molecular Weight Distribution of SRNOM. The molecular weight distribution of pristine-SRNOM was evaluated by determining the dissolved organic carbon (DOC) concentration of each M_f-SRNOM isolated from pristine-SRNOM. The carbon weight proportion (wt%) of each M_f-SRNOM collected after ultrafiltration separation was 7.2 for SRNOM>100, 6.6 for SRNOM30-100, 13.0 for SRNOM10-30, 15.5 for SRNOM3-10, and 57.6 for SRNOM<3, yielding 97.0% recovery of the total pristine-SRNOM DOC. The content of the SRNOM>100 fraction in our study was comparable with the results of Louie et al., in which the SRNOM was separated into MW>100 kD (1.4 wt%) and MW<100 kD (98.6 wt%) fractions,[40] indicating the DOC content of the high MW fraction in SRNOM was much less than the lower MW fraction(s).

Characterization of Pristine- and M_f-SRNOMs. The UV-vis spectra of 10 mg L^{-1} (as carbon) pristine- and M_f-SRNOMs are presented in Figure S1a. The absorbance at 280 nm and the quotient E_2/E_3 (absorbance at 250 and 365 nm), used for estimating the MW-dependent aromaticity of M_f-SRNOMs,[30] were found to be positively and inversely correlated to aromaticity respectively (Figure S1b,c). Of the five fractions, SRNOM>100 and SRNOM30-100 had the highest abundance of aromatic components, indicating the aromatic components and more hydrophobic structures existed mainly in higher M_f-SRNOMs. Furthermore, aromaticity decreased consistently with decreasing MW of the M_f-SRNOM.

For pristine- and M_f-SRNOMs, fluorescence excitation-emission matrices (Figure S2) corrected for the inner-filtering effect, showed that the excitation/emission wavelengths (Ex/Em) of spectra peaks in all samples were primarily in the range 345-360/444-464 (Table S1), indicating the presence of humic-like structures in all SRNOMs.[41] As the MW of the M_f-SRNOMs increased (with the

exception of SRNOM>100), a detectable red-shift (from 444 to 464) of Em maxima was observed owing to the greater abundance of aromatic chromophores,[42, 43] which was generally consistent with results from the UV-vis spectra. Since the humic-like fluorescence is mainly attributed to carboxylic groups,[43] the general increase in the fluorescence maxima with decreased MW in the primary peaks of M_f-SRNOM Ex/Em spectra indicates an increased abundance of carboxylic functional groups with decreasing M_f-SRNOM MW. Similar results have also been observed in the MW-fractionation of soil HA.[44, 45] Additionally, the presence of a secondary peak near 290/322 indicated the appearance of protein-like components,[41] and the correlation between protein-like components and MW of M_f-SRNOMs was similar to that between carboxylic functional groups and MW of M_f-SRNOMs.

Characterization of nC_{60} Nanoparticles. The pristine nC_{60} were spherical-like in shape, with an average diameter of 35.8±0.6 nm determined by TEM (Figure S3). The Z-average hydrodynamic radius of the pristine nC_{60} suspension was 58.2±0.7 nm. The TEM image results and Z-average hydrodynamic radius indicted that some of the nC_{60} was present as individual particles whilst others formed small aggregates. However, the change of nC_{60} radius through the experiment duration was kept within 2 nm of the original measurement. In addition, the pristine nC_{60} was highly negative charged, with an EPM of -3.6±0.1 μmcm/Vs without electrolytes and -2.8±0.2 μmcm/Vs in 1 mmol L^{-1} phosphate buffer. In previous studies, increasingly negative EPMs of nC_{60} were observed as pH was elevated from 2 to 12, implying the surface charge of nC_{60} stemmed from its surface functional groups.[46, 47]

Electrophoretic Mobility in the Absence and Presence of Pristine- and M_f-SRNOMs. The EPM of nC_{60} in the absence of SRNOMs became less negative with increasing electrolyte

201 concentrations (Figure S4), which was ascribed to the charge screening effect,[48, 49] and is consistent
202 with previous studies.[20, 47, 50, 51] In addition, the efficiencies of the electrolytes in decreasing nC_{60}
203 EPM followed the order of $CaCl_2$>$MgCl_2$>>NaCl (Figure S4), and can be attributed to the divalent
204 cations tending to attenuate the electrostatic repulsion by screening the surface charge of nC_{60} more
205 effectively than monovalent cations.[20, 46, 50, 52]

206 Figure 1 shows the EPMs of nC_{60} in the presence of pristine- and M_f-SRNOMs at pH 7.5 and in
207 the presence of NaCl (100 and 500 mmol L^{-1}), $CaCl_2$ (5 and 20 mmol L^{-1}) and $MgCl_2$ (5 and 20
208 mmol L^{-1}), respectively. Generally, the effects of pristine-SRNOM on EPMs of nC_{60} represented an
209 average of the range of values observed for the M_f-SRNOMs. Moreover, detectable and significant
210 variations of nC_{60} EPMs were observed among the different M_f-SRNOM/electrolyte solutions. In the
211 600 and 100 mmol L^{-1} NaCl solutions, EPMs of nC_{60} in the presence of the higher MW SRNOM
212 fractions (>100 and 30-100) were significantly more negative than the EPMs of the SRNOM-free
213 solutions at the corresponding NaCl concentration (Figure 1a). Whilst the trend is more difficult to
214 conclude significantly with the lower MW SRNOM fractions (3-10 and <3), in general the absolute
215 values of EPMs correlated positively with MW of the SRNOM fractions. It is suggested that the
216 observed trend is the result of the higher abundance of aromatic components increases with the MW
217 of M_f-SRNOM. The π-π interaction between M_f-SRNOM and nC_{60} increases significantly, which in
218 turn increases the number of negatively charged functional groups in M_f-SRNOM-nC_{60} association,
219 leading to a more negative EPM. Consequently, as the lower M_f-SRNOMs have a smaller abundance
220 of aromatic components, so their influence on EPM is less.

221 In 5 mmol L^{-1} $CaCl_2$ solutions, EPMs of nC_{60} in the presence of M_f-SRNOMs did not exhibit any
222 statistically significant differences to the EPM of the SRNOM-free solution (Figure 1b). In addition

to electrostatic interaction between Ca^{2+} and negatively charged functional groups, previous studies have indicated that the complexation/cation-bridging effect of Ca^{2+} with carboxylic groups[9, 25, 53] in NOM are significant. The data in this study indicate that the carboxylic acid content of the different M_f-SRNOMs may not be sufficiently to drive a significant change in EPM. EPMs showed no significant change among M_f-SRNOMs at 20 mmol L^{-1} $CaCl_2$ due to the extreme attenuation of nC_{60} surface charge by the high $CaCl_2$ concentration. At both $MgCl_2$ concentration levels, the MW-dependent effect of M_f-SRNOMs on EPMs was not significant (Figure 1c), which could be attributed to the lower formation constant of Mg^{2+} with humic-like materials compared to that of Ca^{2+} [54, 55]. Of the three electrolytes studied, EPM values only appeared to be influenced by a MW-dependent effect of M_f-SRNOMs in the NaCl samples. In the presence of $CaCl_2$ and $MgCl_2$ there was no observable effect from the different M_f-SRNOMs on EPM. In all studies, electrolyte concentration had a significant affect on EPM values, which decreased with increasing electrolyte concentration.

Aggregation Kinetics of nC_{60} in the Absence of SRNOMs. In 1 mmol L^{-1} phosphate or borate buffer, the mean hydrodynamic radius of nC_{60} at pH 7.5 was 60.8±1.1 nm after 2 hours of continuous measurements, with a mean polydispersivity index of 0.16±0.02. This indicates a well dispersion of nC_{60} particles and that no aggregation occurred in the 1 mmol L^{-1} buffer solution during the measurement. The aggregation attachment efficiency (α) profiles of nC_{60} in the absence of SRNOM against $NaCl_2$, $CaCl_2$ and $MgCl_2$ concentration (Figure S5) clearly delineated reaction-limited and diffusion-limited regimes of nC_{60} aggregation. Extrapolation between the two regimes yielded the critical coagulation concentration (CCC) values of 143 mmol L^{-1}, 6.2 mmol L^{-1}, and 8.0 mmol L^{-1} for

245 NaCl, $CaCl_2$ and $MgCl_2$, respectively. The CCC values determined in this study were above the
246 average of those reported for nC_{60} prepared by a solvent exchange method.[9, 50, 56] This was attributed
247 to the high net negative surface charge of nC_{60} prepared in this study, with a zeta-potential (converted
248 by measured EPM using the Smoluchowski equation) of 41.2±1.3 mV.

249 **Aggregation Kinetics in the Presence of SRNOMs.** ***Stability of nC_{60} in the Presence of***
250 ***M_f-SRNOMs with NaCl.*** The effects of pristine- and M_f-SRNOMs on nC_{60} aggregation were first
251 studied with 50-1000 mmol L^{-1} NaCl. This NaCl concentration range represents a broad spectrum of
252 natural water types from freshwater to brackish waters. Representative aggregation profiles of nC_{60}
253 obtained from TR-DLS measurements (500 mmol L^{-1} NaCl with or without SRNOMs, Figure 2a)
254 showed that nC_{60} aggregation was suppressed significantly in the presence of a relatively low
255 concentration of pristine- and M_f-SRNOMs (1 mg L^{-1}). Similar results have also been observed for
256 rotavirus[49], nC_{60}[9, 56] and CNTs[57] in the presence of unfractionated NOMs. The α values of nC_{60} in the
257 presence of 1 mg L^{-1} SRNOMs were plotted as a function of NaCl concentration in Figure 3. As
258 shown in Figures 3, 4a and 4c, the addition of any M_f-SRNOM resulted in an elevated CCC value
259 compared with that in SRNOM-free solutions (1.06 to 4.15 times), and the increment of CCC
260 positively correlated to MW of M_f-SRNOMs. In addition, the CCC for nC_{60} in pristine-SRNOM
261 solutions occurred at 167 mmol L^{-1} NaCl. This is 1.17 times higher than that observed in the
262 SRNOM-free solutions and similar to that observed in SRNOM3-10 (163 mmol L^{-1}). Therefore, this
263 values falls in the medium range of the CCC values determined the in M_f-SRNOMs solutions. To
264 investigate the stability of nC_{60} in high concentration electrolytes, the mean α values of nC_{60} in
265 diffusion-limited regimes in pristine- and M_f-SRNOM NaCl solutions were compared with those for
266 SRNOM-free solutions (Figure 4b). At an identical NaCl concentration, the addition of SRNOMs

generally suppressed the α values compared with those for SRNOM-free solutions, and the α values were inversely correlated with the MW of the M_f-SRNOMs.

Over the NaCl concentration range studied, the attenuation of α values revealed that the presence of pristine- and M_f-SRNOMs enhanced the stability of nC_{60}. The aggregation kinetics clearly showed that nC_{60} stability was positively correlated to the MW of the M_f-SRNOMs. These observations strongly indicated that a MW-dependent steric-hindrance effect[16] was the most important mechanism responsible for the stability of nC_{60} in solutions of NaCl/SRNOMs. In addition, the greater abundance of aromatic components in higher M_f-SRNOMs were expected to increase their adsorption strength to nC_{60} through π-π interactions[58], and therefore enhance the nC_{60} stability. Therefore, the steric hindrance effect appears to be a combination of increased adsorption and the larger abundance of aromatic components in the higher MW fractions. Moreover, because of the absence of a cation-bridging effect and relatively weaker electrostatic interaction between Na^+ and M_f-SRNOMs, the adsorption of higher M_f-SRNOMs contributed more to the negatively charged M_f-SRNOM-nC_{60} association and therefore the nC_{60} stability. In addition, the decreased aggregation observed for the higher M_f-SRNOMs is also due to the greater negative surface charge caused by the higher NOM adsorption.

Suppressed Aggregation in the Presence of SRNOMs and Low Concentrations of $CaCl_2$ or $MgCl_2$. The aggregation kinetics of nC_{60} were also examined in the divalent electrolytes $CaCl_2$ and $MgCl_2$. Figures 5 and 6 show the α values of nC_{60} as a function of $CaCl_2$ and $MgCl_2$ concentration, respectively. In general,

289 SRNOMs suppressed the aggregation of nC_{60} at low $CaCl_2$ and $MgCl_2$ concentrations, which was
290 attributed to the additionally promoted instability of SRNOM-nC_{60} association by
291 complexation/cation-bridging effects between Ca^{2+}(Mg^{2+}) and SRNOMs. It should be noted that the
292 aggregation suppression of $CaCl_2$ and $MgCl_2$ occurred to lesser extent than that exhibited at low
293 NaCl concentrations. In addition, the profile of the reaction-limited regime shifted to the right with
294 the increase of MW of the M_f-SRNOMs, indicating M_f-SRNOMs with higher MW were more
295 efficient in stabilizing nC_{60} at low divalent electrolyte concentrations. It is noteworthy that this
296 SRNOM-MW-dependent right shift for $MgCl_2$ was more significant than that for $CaCl_2$. Overall, the
297 efficiencies of Mf-SRNOMs on stabilizing nC_{60} in three cations followed an order of
298 NaCl>$MgCl_2$>$CaCl_2$.

299 To further evaluate the suppression efficiency, the electrolyte concentrations at α=0.01 in
300 SRNOMs were normalized to that of the SRNOM-free solution (referred as $Q_{\alpha=0.01}$). To this end, the
301 α values in reaction-limited regimes were linearly correlated to the concentrations of the three
302 electrolytes in logarithmic coordinates, and the electrolyte concentrations at α=0.01 were calculated.
303 From the $Q_{\alpha=0.01}$ values for the three electrolyte solutions (Figure 4d), it was clear that
304 pristine-SRNOM was slightly more effective in stabilizing nC_{60} in $MgCl_2$, than in $CaCl_2$ and NaCl.
305 However, different effects were observed for different M_f-SRNOMs. First, the stabilization of nC_{60}
306 in any of the three electrolyte solutions was correlated positively with the MW of SRNOMs, and was
307 most enhanced by SRNOM>100, following an order of NaCl>$MgCl_2$>$CaCl_2$. Second, however, the
308 distinction among stabilization efficiencies of various M_f-SRNOMs on nC_{60} aggregation was greatest
309 in NaCl solutions and least in $CaCl_2$ solutions. Noticeably, for the low M_f-SRNOMs (SRNOM3-10
310 and SRNOM<3), except $CaCl_2$/SRNOM3-10 where no significant change of nC_{60} aggregation was

311 observed compared with that in $CaCl_2$/SRNOM-free solution, all three electrolytes did not retard but
312 actually enhanced the aggregation of nC_{60}.

313 ***Enhanced Aggregation in the Presence of SRNOMs and High Concentrations of $CaCl_2$ or***
314 ***$MgCl_2$.*** The effects of high concentration divalent electrolytes on the aggregation kinetics of nC_{60} is
315 complicated in the presence of SRNOMs (Figures 2b,c, 5 and 6). As shown in Figures 5 and 4c, the
316 CCC for nC_{60} in the mixture of pristine-SRNOM and $CaCl_2$ solution was 1.22 times that in $CaCl_2$
317 solutions. The CCC values increased with the MW of M_f-SRNOMs, which were 1.02 to 1.80 times
318 of those in the corresponding SRNOM-free solutions. However, the apparent changes in CCC values
319 induced by the MW of M_f-SRNOMs in $MgCl_2$ solutions were greater than those in $CaCl_2$ solutions
320 (Figures 4c, 5 and 6). Except for a lower CCC value (7.3 mmol L^{-1}) in SRNOM<3 compared to that
321 in the SRNOM-free solutions (8.0 mmol L^{-1}), the CCC values for nC_{60} in the other
322 M_f-SRNOM/$MgCl_2$ solutions increased with the increasing MW of M_f-SRNOM and were 1.13 to
323 3.22 times that observed for the corresponding SRNOM-free solutions.

324 To further investigate the effects of SRNOMs on the aggregation of nC_{60} at high divalent
325 electrolyte concentrations, the calculated α values of nC_{60} at CCC in SRNOMs/$CaCl_2$ solutions were
326 compared with those in SRNOM-free solutions. Except for the extremely high α value of 0.78
327 observed in SRNOM>100, all other α values at CCC increased with decreasing MW of M_f-SRNOMs.
328 The lowest of 0.57 was observed in SRNOM30-100 and highest value of 0.79 in SRNOM<3. The α
329 value at CCC in $CaCl_2$ solutions was much higher than that in NaCl solutions, indicating
330 M_f-SRNOMs had much weaker capability for stabilizing nC_{60} in $CaCl_2$ than in NaCl solutions. A
331 similar phenomenon was also observed for unfractionated SRHA in stabilizing nC_{60} in NaCl and
332 $CaCl_2$.[9]

333 However, when the $CaCl_2$ concentration exceeded CCC values, the aggregation kinetics in the
334 SRNOM solutions were generally dependent on the $CaCl_2$ concentration, which is comparable to that
335 observed in the SRNOM-free solutions. In contrast, α values in most SRNOMs kept on increasing
336 with $CaCl_2$ concentration (Figure 5). In the presence of pristine-SRNOM, the α value finally
337 plateaued at 0.76±0.05 for $CaCl_2$ concentrations ≥20 mmol L^{-1}. Although the aggregation rate of nC_{60}
338 in pristine-SRNOM/$CaCl_2$ did not exceed that in SRNOM-free/$CaCl_2$ solutions (α<1), an enhanced
339 aggregation of nC_{60} was still observed. In a previous study, Chen et al. report a comparable result
340 following the addition of 1 mg L^{-1} unfractionated SRHA and ≥15 mmol L^{-1} $CaCl_2$, which led to an
341 enhanced aggregation of nC_{60} (α>1).[9] The smaller α value in the present study could be attributed to
342 the smaller MW and reduced aromaticity of SRNOM than that of SRHA.[55, 59] In addition to a
343 specific enhancement of nC_{60} aggregation in SRNOM<3/30 mmol L^{-1} $CaCl_2$ (α=1.18±0.12), the most
344 enhanced or accelerated aggregation kinetics of nC_{60} occurred in the SRNOM>100 and
345 SRNOM30-100 solutions, with respective α values of 1.17±0.10 and 0.93±0.06 at $CaCl_2$
346 concentrations over 20 mmol L^{-1}. From the highest to the lowest MW of M_f-SRNOM, the final
347 steady states of α values followed a V-shaped trend, with the most retarded one occurring in the
348 SRNOM10-30 solutions (α=0.73±0.05 at $CaCl_2$ concentration >15 mmol L^{-1}). Evidence for humic
349 aggregation in electrolytes has been observed previously.[35, 53, 60]

350 The adsorption of the different M_f-SRNOM changes the final composition of the particles nC_{60}.
351 The lowest MW fractions have the lowest fraction of aromatic groups and therefore adsorb the least
352 to the nC_{60}, while the highest MW fractions have the highest fraction of aromatic groups and
353 therefore adsorb the most. This impacts the surface charge in different situations XX. Furthermore,
354 this also affects the thickness of the electrolyte layer on the particles. It is this combination of

355 adsorption of specific M_f-SRNOMs and interaction with the electrolyte layer which determines the
356 final stability of the nC_{60} particles.

357 In M_f-SRNOMs/$MgCl_2$ solutions with $MgCl_2$ concentration over CCC for nC_{60}, the
358 concentration-dependent increase of α values only occurred in SRNOM>100 and SRNOM30-100
359 solutions. However, the α values were below 1 even at 70 mmol L^{-1} $MgCl_2$ even though the
360 aggregation kinetics of nC_{60} in the two M_f-SRNOMs were accelerated. It has previously been
361 reported that Mg^{2+} has a lower formation constant with humic-like materials than Ca^{2+},[54] and that the
362 smaller Mg^{2+} ion (compared to Ca^{2+}) results in an interaction with fewer SRHA-coated ENPs.[55]
363 Accordingly, the weaker complexation/cation-bridging between $MgCl_2$ and M_f-SRNOMs means that
364 only the most humic-like fractions (SRNOM>100 and SRNOM30-100) in the present study were
365 able to enhancing aggregation kinetics of nC_{60} at high $MgCl_2$ concentrations.

366 Overall, the interactions among cations, M_f-SRNOMs and nC_{60} invoked different mechanisms, and
367 the impacts of M_f-SRNOMs on nC_{60} aggregation changed significantly with both NOM MW and
368 cation species. The main mechanisms responsible for nC_{60} aggregation are (1) steric-hindrance
369 effects of M_f-SRNOM on stabilizing nC_{60}, which was elevated with the enhanced adsorption of
370 M_f-SRNOMs on nC_{60} and larger molecular size when MW increased; (2) the
371 complexation/cation-bridging effects between M_f-SRNOM and Ca^{2+}(Mg^{2+}), which were responsible
372 for EPM attenuation and larger but less stable networks of bridged M_f-SRNOM molecules, thus
373 promoting homoaggregation of M_f-SRNOM-nC_{60} association at higher Ca^{2+} (Mg^{2+}) concentrations.
374 It is interesting to note that, (1) M_f-SRNOMs with extremely high MW enabled not only enhanced
375 adsorption to nC_{60} but also stronger interaction with cations, which resulted in cation
376 species-dependent nC_{60} aggregation; (2) although the lowest M_f-SRNOM had the weakest capability

377 in stabilizing nC_{60} due to a lower steric-hindrance ability, the abundant carboxylic groups gave rise to
378 stronger complexation with Ca^{2+} and therefore elevated aggregation kinetics of nC_{60}; (3)
379 steric-hindrance effects of M_f-SRNOMs are always present, but was most important at low
380 electrolyte concentrations; (4) complexation/cation-bridging-induced homoaggregation of
381 M_f-SRNOM-nC_{60} was mostly observed at high Ca^{2+}(Mg^{2+}) concentrations, but also resulted in less
382 stable M_f-SRNOM-nC_{60} association at low Ca^{2+}(Mg^{2+}) concentrations.

383

384 This study has provided an insight into the fate and transport of fullerenes in aqueous environments.
385 Key aspects in the mechanism governing the initial aggregation kinetics of nC_{60} changed
386 significantly with the MW and physicochemical properties of M_f-SRNOMs, varied among cations,
387 and differed under low to high concentrations of electrolyte solutions. Therefore, the aggregation and
388 even deposition of ENPs affected by NOM and cations are very likely to influence the ENP
389 distribution between sediment-water interface, which ultimately have impacts on uptake and
390 therefore bioavailability and toxicity of ENPs to organisms in aqueous environment.

391

392 **ASSOCIATED CONTENT**

393 **Supporting Information**

394 Experimental details of the spectroscopic characterization of pristine-, M_f-SRNOMs and nC_{60}, C_{60}
395 concentration determination, electrophoretic mobility measurements, aggregation kinetics of nC_{60} by
396 Time resolved DLS, and results of pristine-, M_f-SRNOMs and nC_{60} characterization, EPMs and
397 aggregation studies of nC_{60} are provided in Supporting Information. This material is available free of
398 charge *via* the Internet at http://pubs.acs.org.

AUTHOR INFORMATION

Corresponding Author

* Tel.: +86-10-62849192; Fax: +86-10-62849192; E-mail: jfliu@rcees.ac.cn.

ACKNOWLEDGMENTS

This research was funded by the National Basic Research Program of China (2010CB933502), External Cooperation Program of Chinese Academy of Sciences (GJHZ1206), the National Natural Science Foundation of China (21025729, 21337004), and the Norwegian Research Council (grant number 209685).

REFERENCES

(1) Liu, J. F.; Yu, S. J.; Yin, Y. G.; Chao, J. B. Methods for separation, identification, characterization and quantification of silver nanoparticles. *Trends Anal. Chem.* **2012,** *33*, 95-106.

(2) Mauter, M. S.; Elimelech, M. Environmental applications of carbon-based nanomaterials. *Environ. Sci. Technol.* **2008,** *42* (16), 5843-5859.

(3) The Project on Emerging Technologies, http://www.nanotechproject.org/inventories/consumer/analysis_draft/. (Accessed on October 30, 2013),

(4) Jehlicka, J.; Frank, O.; Hamplova, V.; Pokorna, Z.; Juha, L.; Bohacek, Z.; Weishauptova, Z. Low extraction recovery of fullerene from carbonaceous geological materials spiked with C_{60}. *Carbon* **2005,** *43* (9), 1909-1917.

(5) Murr, L. E.; Soto, K. F. A TEM study of soot, carbon nanotubes, and related fullerene nanopolyhedra in common fuel-gas combustion sources. *Mater. Charact.* **2005,** *55* (1), 50-65.

(6) Jafvert, C. T.; Kulkarni, P. P. Buckminsterfullerene's (C_{60}) octanol-water partition coefficient (K_{ow}) and aqueous solubility. *Environ. Sci. Technol.* **2008,** *42* (16), 5945-5950.

(7) Brant, J. A.; Labille, J.; Bottero, J. Y.; Wiesner, M. R. Characterizing the impact of preparation method on fullerene cluster structure and chemistry. *Langmuir* **2006,** *22* (8), 3878-3885.

(8) Ma, X.; Bouchard, D. Formation of aqueous suspensions of fullerenes. *Environ. Sci. Technol.* **2009,** *43* (2), 330-336.

(9) Chen, K. L.; Elimelech, M. Influence of humic acid on the aggregation kinetics of fullerene (C_{60}) nanoparticles in monovalent and divalent electrolyte solutions. *J. Colloid. Interf. Sci.* **2007,** *309* (1), 126-134.

(10) Henry, T. B.; Petersen, E. J.; Compton, R. N. Aqueous fullerene aggregates (nC_{60}) generate minimal reactive oxygen species and are of low toxicity in fish: a revision of previous reports. *Curr. Opin. Biotech.* **2011,** *22* (4), 533-537.

(11) Aschberger, K.; Johnston, H. J.; Stone, V.; Aitken, R. J.; Tran, C. L.; Hankin, S. M.; Peters, S. A. K.; Christensen, F. M. Review of fullerene toxicity and exposure - Appraisal of a human health risk assessment, based on open literature. *Regul. Toxicol. Pharm.* **2010,** *58* (3), 455-473.

(12) Kolosnjaj, J.; Smarc, H.; Moussa, F. Toxicity studies of fullerenes and derivatives. *Adv. Exp. Med. Biol.* **2007,** *620*, 168-180.

(13) Baun, A.; Sorensen, S. N.; Rasmussen, R. F.; Hartmann, N. B.; Koch, C. B. Toxicity and bioaccumulation of xenobiotic organic compounds in the presence of aqueous suspensions of aggregates of nano-C_{60}. *Aquat. Toxicol.* **2008,** *86* (3), 379-387.

(14) Lowry, G. V.; Gregory, K. B.; Apte, S. C.; Lead, J. R. Transformations of nanomaterials in the environment. *Environ. Sci. Technol.* **2012,** *46* (13), 6893-6899.

(15) Klaine, S. J.; Alvarez, P. J. J.; Batley, G. E.; Fernandes, T. F.; Handy, R. D.; Lyon, D. Y.; Mahendra, S.; McLaughlin, M. J.; Lead, J. R. Nanomaterials in the environment: Behavior, fate, bioavailability, and effects. *Environ. Toxicol. Chem.* **2008,** *27* (9), 1825-1851.

(16) Petosa, A. R.; Jaisi, D. P.; Quevedo, I. R.; Elimelech, M.; Tufenkji, N. Aggregation and deposition of engineered nanomaterials in aquatic environments: Role of physicochemical interactions. *Environ. Sci. Technol.* **2010,** *44* (17), 6532-6549.

(17) Zhang, Y.; Chen, Y. S.; Westerhoff, P.; Crittenden, J. Impact of natural organic matter and divalent cations on the stability of aqueous nanoparticles. *Water Res.* **2009,** *43* (17), 4249-4257.

(18) Liu, J.; Legros, S.; Von der Kammer, F.; Hofmann, T. Natural organic matter concentration and hydrochemistry influence aggregation kinetics of functionalized engineered nanoparticles. *Environ. Sci. Technol.* **2013,** *47* (9), 4113-4120.

(19) Xie, B.; Xu, Z. H.; Guo, W. H.; Li, Q. L. Impact of natural organic matter on the physicochemical properties of aqueous C_{60} nanoparticles. *Environ. Sci. Technol.* **2008,** *42* (8), 2853-2859.
(20) Zhang, W.; Rattanaudompol, U. S.; Li, H.; Bouchard, D. Effects of humic and fulvic acids on aggregation of aqu/nC_{60} nanoparticles. *Water Res.* **2013,** *47* (5), 1793-802.
(21) Hyung, H.; Kim, J. H. Natural organic matter (NOM) adsorption to multi-walled carbon nanotubes: Effect of NOM characteristics and water quality parameters. *Environ. Sci. Technol.* **2008,** *42* (12), 4416-4421.
(22) Saleh, N. B.; Pfefferle, L. D.; Elimelech, M. Aggregation kinetics of multiwalled carbon nanotubes in aquatic systems: Measurements and environmental implications. *Environ. Sci. Technol.* **2008,** *42* (21), 7963-7969.
(23) Lin, D.; Xing, B. Tannic acid adsorption and its role for stabilizing carbon nanotube suspensions. *Environ. Sci. Technol.* **2008,** *42* (16), 5917-5923.
(24) Isaacson, C. W.; Bouchard, D. C. Effects of humic acid and sunlight on the generation and aggregation state of aqu/C_{60} nanoparticles. *Environ. Sci. Technol.* **2010,** *44* (23), 8971-8976.
(25) Qu, X.; Hwang, Y. S.; Alvarez, P. J. J.; Bouchard, D.; Li, Q. UV irradiation and humic acid mediate aggregation of aqueous fullerene (nC_{60}) nanoparticles. *Environ. Sci. Technol.* **2010,** *44* (20), 7821-7826.
(26) Terashima, M.; Nagao, S. Solubilization of [60]fullerene in water by aquatic humic substances. *Chem. Lett.* **2007,** *36* (2), 302-303.
(27) Chen, K. L.; Smith, B. A.; Ball, W. P.; Fairbrother, D. H. Assessing the colloidal properties of engineered nanoparticles in water: case studies from fullerene C_{60} nanoparticles and carbon nanotubes. *Environ. Chem.* **2010,** *7* (1), 10-27.
(28) Chen, J.; Gu, B. H.; LeBoeuf, E. J.; Pan, H. J.; Dai, S. Spectroscopic characterization of the structural and functional properties of natural organic matter fractions. *Chemosphere* **2002,** *48* (1), 59-68.
(29) Schafer, A. I.; Mauch, R.; Waite, T. D.; Fane, A. G. Charge effects in the fractionation of natural organics using ultrafiltration. *Environ. Sci. Technol.* **2002,** *36* (12), 2572-2580.
(30) Peuravuori, J.; Pihlaja, K. Molecular size distribution and spectroscopic properties of aquatic humic substances. *Anal. Chim. Acta* **1997,** *337* (2), 133-149.
(31) Her, N.; Amy, G.; McKnight, D.; Sohn, J.; Yoon, Y. M. Characterization of DOM as a function of MW by fluorescence EEM and HPLC-SEC using UVA, DOC, and fluorescence detection. *Water Res.* **2003,** *37* (17), 4295-4303.
(32) Li, L.; Zhao, Z. Y.; Huang, W. L.; Peng, P.; Sheng, G. Y.; Fu, J. M. Characterization of humic acids fractionated by ultrafiltration. *Org. Geochem.* **2004,** *35* (9), 1025-1037.
(33) Sharpless, C. M. Lifetimes of triplet dissolved natural organic matter (DOM) and the effect of NaBH4 reduction on singlet oxygen quantum yields: Implications for DOM photophysics. *Environ. Sci. Technol.* **2012,** *46* (8), 4466-4473.
(34) Piccolo, A. The supramolecular structure of humic substances. *Soil. Sci.* **2001,** *166* (11), 810-832.
(35) Baalousha, M.; Motelica-Heino, M.; Le Coustumer, P. Conformation and size of humic substances: Effects of major cation concentration and type, pH, salinity, and residence time. *Colloids Surf., A* **2006,** *272* (1-2), 48-55.
(36) Christl, I.; Kretzschmar, R. Relating ion binding by fulvic and humic acids to chemical composition and molecular size. 1. Proton binding. *Environ. Sci. Technol.* **2001,** *35* (12), 2505-2511.
(37) Christl, I.; Milne, C. J.; Kinniburgh, D. G.; Kretzschmar, R. Relating ion binding by fulvic and humic acids to chemical composition and molecular size. 2. Metal binding. *Environ. Sci. Technol.* **2001,** *35* (12), 2512-2517.
(38) Kalinichev, A. G.; Iskrenova-Tchoukova, E.; Ahn, W.-Y.; Clark, M. M.; Kirkpatrick, R. J. Effects of Ca^{2+} on supramolecular aggregation of natural organic matter in aqueous solutions: A comparison of molecular modeling approaches. *Geoderma* **2011,** *169*, 27-32.
(39) Kloster, N.; Brigante, M.; Zanini, G.; Avena, M. Aggregation kinetics of humic acids in the presence of

calcium ions. *Colloids Surf., A* **2013,** *427*, 76-82.
(40) Louie, S. M.; Tilton, R. D.; Lowry, G. V. Effects of molecular weight distribution and chemical properties of natural organic matter on gold nanoparticle aggregation. *Environ. Sci. Technol.* **2013,** *47* (9), 4245-54.
(41) Hudson, N.; Baker, A.; Reynolds, D. Fluorescence analysis of dissolved organic matter in natural, waste and polluted waters - A review. *River. Res. Appl.* **2007,** *23* (6), 631-649.
(42) Sierra, M. M. D.; Giovanela, M.; Parlanti, E.; Soriano-Sierra, E. J. Fluorescence fingerprint of fulvic and humic acids from varied origins as viewed by single-scan and excitation/emission matrix techniques. *Chemosphere* **2005,** *58* (6), 715-733.
(43) Wu, F. C.; Evans, R. D.; Dillon, P. J. Separation and characterization of NOM by high-performance liquid chromatography and on-line three-dimensional excitation emission matrix fluorescence detection. *Environ. Sci. Technol.* **2003,** *37* (16), 3687-3693.
(44) Richard, C.; Trubetskaya, O.; Trubetskoj, O.; Reznikova, O.; Afanas'eva, G.; Aguer, J. P.; Guyot, G. Key role of the low molecular size fraction of soil humic acids for fluorescence and photoinductive activity. *Environ. Sci. Technol.* **2004,** *38* (7), 2052-2057.
(45) Richard, C.; Guyot, G.; Rivaton, A.; Trubetskaya, O.; Trubetskoj, O.; Cavani, L.; Ciavatta, C. Spectroscopic approach for elucidation of structural peculiarities of Andisol soil humic acid fractionated by SEC-PAGE setup. *Geoderma* **2007,** *142* (1-2), 210-216.
(46) Brant, J.; Lecoanet, H.; Hotze, M.; Wiesner, M. Comparison of electrokinetic properties of colloidal fullerenes (n-C_{60}) formed using two procedures. *Environ. Sci. Technol.* **2005,** *39* (17), 6343-6351.
(47) Chen, K. L.; Elimelech, M. Relating colloidal stability of fullerene (C_{60}) nanoparticles to nanoparticle charge and electrokinetic properties. *Environ. Sci. Technol.* **2009,** *43* (19), 7270-7276.
(48) Yi, P.; Chen, K. L. Influence of surface oxidation on the aggregation and deposition kinetics of multiwalled carbon nanotubes in monovalent and divalent electrolytes. *Langmuir* **2011,** *27* (7), 3588-3599.
(49) Gutierrez, L.; Nguyen, T. H. Interactions between rotavirus and suwannee river organic matter: Aggregation, deposition, and adhesion force measurement. *Environ. Sci. Technol.* **2012,** *46* (16), 8705-8713.
(50) Chen, K. L.; Elimelech, M. Aggregation and deposition kinetics of fullerene (C_{60}) nanoparticles. *Langmuir* **2006,** *22* (26), 10994-11001.
(51) Yang, Y.; Nakada, N.; Nakajima, R.; Yasojima, M.; Wang, C.; Tanaka, H. pH, ionic strength and dissolved organic matter alter aggregation of fullerene C_{60} nanoparticles suspensions in wastewater. *J. Hazard. Mater.* **2013,** *244*, 582-587.
(52) Mukherjee, B.; Weaver, J. W. Aggregation and charge behavior of metallic and nonmetallic nanoparticles in the presence of competing similarly-charged inorganic ions. *Environ. Sci. Technol.* **2010,** *44* (9), 3332-3338.
(53) Wang, L.-F.; Wang, L.-L.; Ye, X.-D.; Li, W.-W.; Ren, X.-M.; Sheng, G.-P.; Yu, H.-Q.; Wang, X.-K. Coagulation kinetics of humic aggregates in mono- and di-valent electrolyte solutions. *Environ. Sci. Technol.* **2013,** *47* (10), 5042-9.
(54) Tipping, E.; Hurley, M. A. A unifying model of cation binding by humic substances. *Geochim. Cosmochim. Acta* **1992,** *56* (10), 3627-3641.
(55) Akaighe, N.; Depner, S. W.; Banerjee, S.; Sharma, V. K.; Sohn, M. The effects of monovalent and divalent cations on the stability of silver nanoparticles formed from direct reduction of silver ions by Suwannee River humic acid/natural organic matter. *Sci. Total Environ.* **2012,** *441*, 277-289.
(56) Meng, Z.; Hashmi, S. M.; Elimelech, M. Aggregation rate and fractal dimension of fullerene nanoparticles via simultaneous multiangle static and dynamic light scattering measurement. *J. Colloid. Interf. Sci.* **2013,** *392*, 27-33.
(57) Saleh, N. B.; Pfefferle, L. D.; Elimelech, M. Influence of biomacromolecules and humic acid on the aggregation kinetics of single-walled carbon nanotubes. *Environ. Sci. Technol.* **2010,** *44* (7), 2412-2418.

(58) Mashayekhi, H.; Ghosh, S.; Du, P.; Xing, B. Effect of natural organic matter on aggregation behavior of C_{60} fullerene in water. *J. Colloid. Interf. Sci.* **2012,** *374*, 111-117.

(59) International Humic Substances Society, http://www.humicsubstances.org/. (Accessed on October 30, 2013),

(60) Tamamura, S.; Ohashi, R.; Nagao, S.; Yamamoto, M.; Mizuno, M. Molecular-size-distribution-dependent aggregation of humic substances by Na(I), Ag(I), Ca(II), and Eu(III). *Colloids Surf., A* **2013,** *434*, 9-15.

(61) Chen, W. B.; Smith, D. S.; Gueguen, C. Influence of water chemistry and dissolved organic matter (DOM) molecular size on copper and mercury binding determined by multiresponse fluorescence quenching. *Chemosphere* **2013,** *92* (4), 351-359.

(62) Thurman, E. M. *Organic geochemistry of natural waters*; Martinus Nijhoff/Dr W. Junk Publishers: Dordrecht, 1985.

(63) Song, M.; Yuan, S.; Yin, J.; Wang, X.; Meng, Z.; Wang, H.; Jiang, G. Size-dependent toxicity of nano-C_{60} aggregates: more sensitive indication by apoptosis-related bax translocation in cultured human cell. *Environ. Sci. Technol.* **2012,** *46* (6), 3457-3464.

FIGURE CAPTIONS

Figure 1. EPMs of nC_{60} in the absence and presence of SRNOMs in (a) 100 and 500 mmol L^{-1} NaCl, (b) 5 and 20 mmol L^{-1} $CaCl_2$ and (c) 5 and 20 mmol L^{-1} $MgCl_2$ solutions. The error bars represent the standard deviation from 6-12 measurements of 2-4 samples.

Figure 2. Time resolved z-average hydrodynamic radii for nC_{60} in (a) 500 mmol L^{-1} NaCl, 1 mmol L^{-1} phosphate buffer, pH 7.5; (b) 20 mmol L^{-1} $CaCl_2$, 1 mmol L^{-1} borate buffer, pH 7.5; and (c) 20 mmol L^{-1} $MgCl_2$, 1 mmol L^{-1} borate buffer, pH 7.5, in the absence and presence of 1 mgL^{-1} of pristine- and M_f-SRNOMs. Error bars are standard deviations computed for z-average hydrodynamic radii from triplicate samples at the same solution chemistry. It should be noted that, although radii data within 11 min were used in this figure, enough radii data ($R_h(t) \geq 1.25 R_h(0)$) were recorded for calculation of the initial aggregation rate constant.

Figure 3. Attachment efficiency values of nC_{60} as a function of NaCl concentration in the presence of pristine-SRNOM and M_f-SRNOMs. Data for "no SRNOM" (□) solutions are also given in (a, b) to facilitate the comparison of differences of α values among no SRNOM, pristine- and M_f-SRNOM solutions. The error bars represent the standard deviation from triplicate samples. The dashed lines represent a visual guide to distinguish the reaction-limited and diffusion-limited regimes.

Figure 4. (a) Critical coagulation concentration (CCC) values of NaCl for nC_{60} in the absence and presence of pristine- or M_f-SRNOMs; (b) The mean attachment efficiency (α) values of nC_{60}, in the absence and presence of pristine- and M_f-SRNOMs in the diffusion-limited regimes, in monovalent

electrolyte NaCl (error bars represent the standard deviation from triplicate samples); (c) CCC for the three electrolytes in the presence of pristine- or M_f-SRNOMs normalized to that in the absence of SRNOMs; (d) Electrolyte concentrations at α=0.01 in the presence of pristine- and M_f-SRNOMs normalized to that in the absence of SRNOMs ($Q_{\alpha=0.01}$).

Figure 5. Attachment efficiency values of nC_{60} as a function of $CaCl_2$ concentration in the presence of pristine-SRNOM and M_f-SRNOMs. The symbol statements are the same as in Figure 4.

Figure 6. Attachment efficiency values of nC_{60} as a function of $MgCl_2$ concentration in the presence of pristine-SRNOM and M_f-SRNOMs. The symbol statements are the same as in Figure 4.

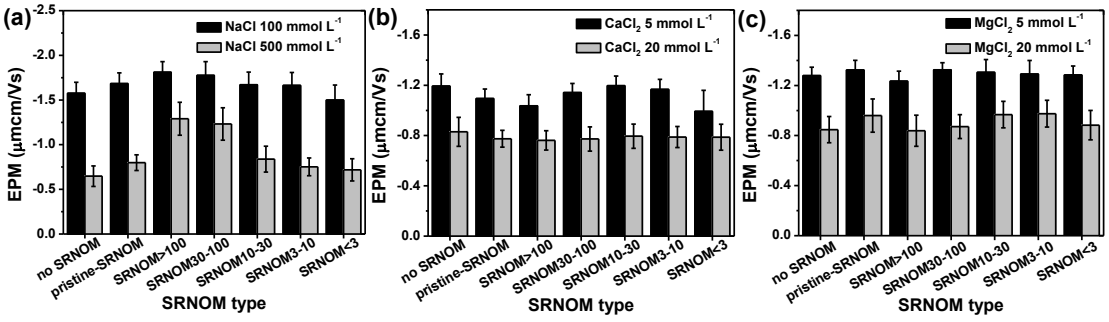

Figure 1. EPMs of nC_{60} in the absence and presence of SRNOMs in (a) 100 and 500 mmol L^{-1} NaCl, (b) 5 and 20 mmol L^{-1} $CaCl_2$ and (c) 5 and 20 mmol L^{-1} $MgCl_2$ solutions. The error bars represent the standard deviation from 6-12 measurements of 2-4 samples.

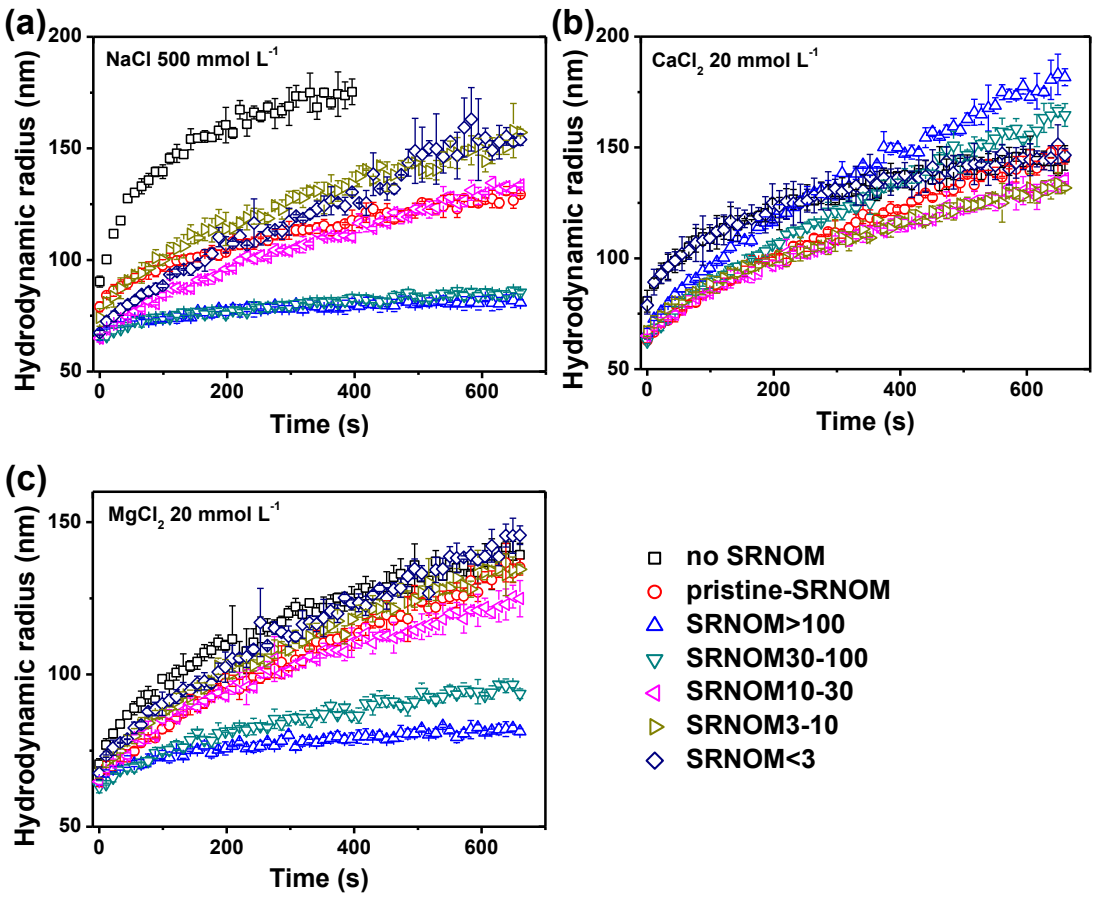

Figure 2. Time resolved z-average hydrodynamic radii for nC_{60} in (a) 500 mmol L^{-1} NaCl, 1 mmol L^{-1} phosphate buffer, pH 7.5; (b) 20 mmol L^{-1} $CaCl_2$, 1 mmol L^{-1} borate buffer, pH 7.5; and (c) 20 mmol L^{-1} $MgCl_2$, 1 mmol L^{-1} borate buffer, pH 7.5, in the absence and presence of 1 mgL^{-1} of pristine- and M_f-SRNOMs. Error bars are standard deviations computed for z-average hydrodynamic radii from triplicate samples at the same solution chemistry. It should be noted that, although radii data within 11 min were used in this figure, enough radii data ($R_h(t) \geq 1.25 R_h(0)$) were recorded for calculation of the initial aggregation rate constant.

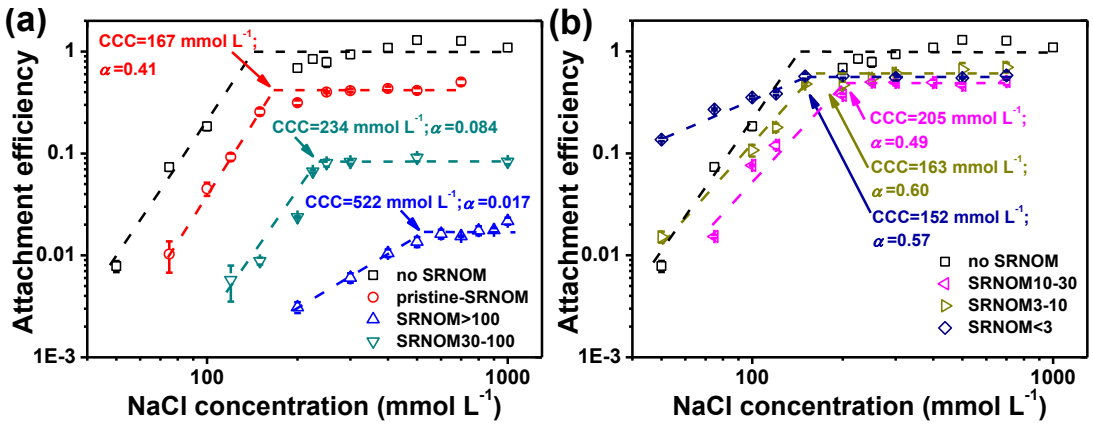

Figure 3. Attachment efficiency values of nC_{60} as a function of NaCl concentration in the presence of pristine-SRNOM and M_f-SRNOMs. Data for "no SRNOM" (□) solutions are also given in (a, b) to facilitate the comparison of differences of α values among no SRNOM, pristine- and M_f-SRNOM solutions. The error bars represent the standard deviation from triplicate samples. The dashed lines represent a visual guide to distinguish the reaction-limited and diffusion-limited regimes.

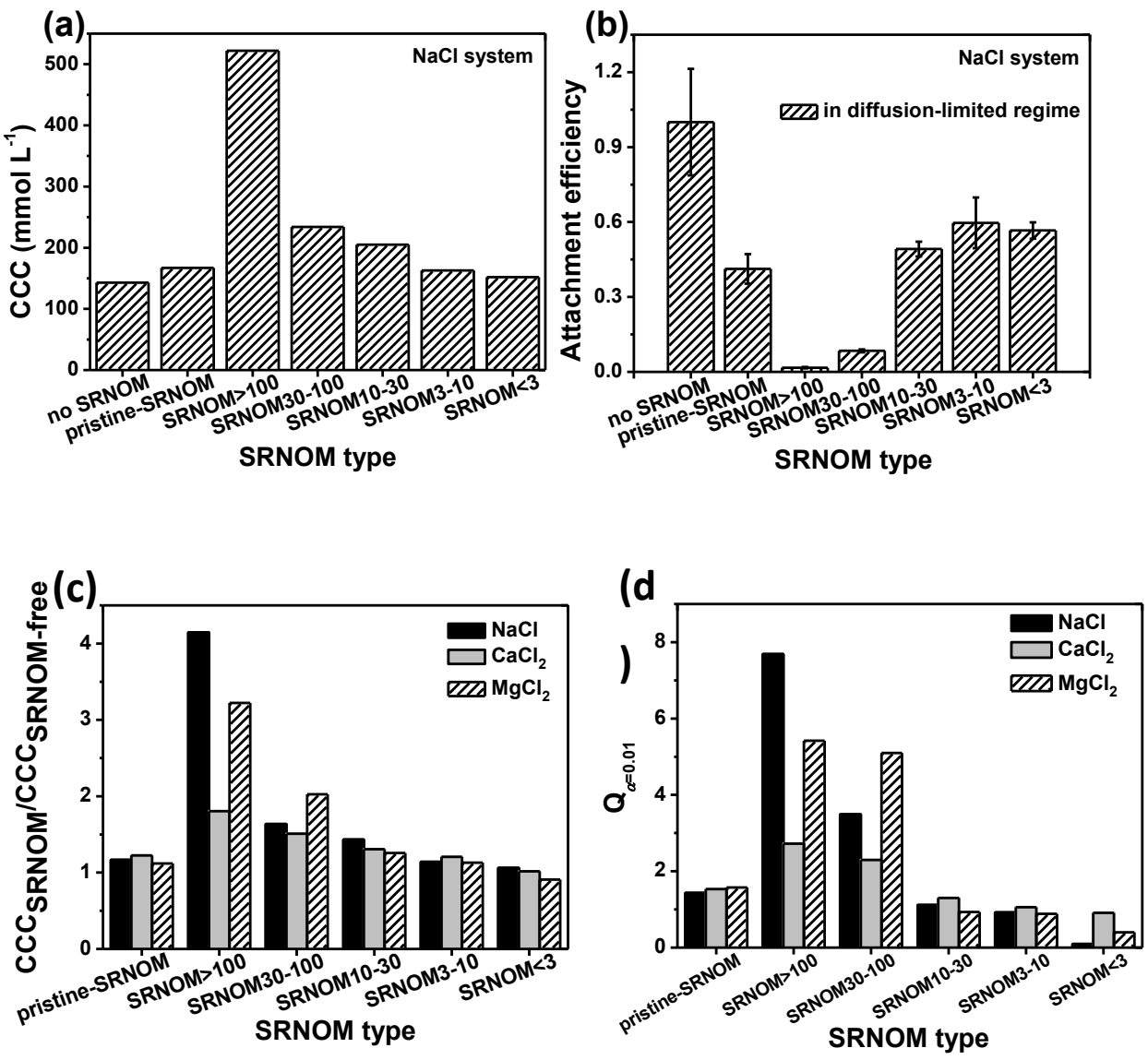

Figure 4. (a) Critical coagulation concentration (CCC) values of NaCl for nC_{60} in the absence and presence of pristine- or M_f-SRNOMs; (b) The mean attachment efficiency (α) values of nC_{60}, in the absence and presence of pristine- and M_f-SRNOMs in the diffusion-limited regimes, in monovalent electrolyte NaCl (error bars represent the standard deviation from triplicate samples); (c) CCC for the three electrolytes in the presence of pristine- or M_f-SRNOMs normalized to that in the absence of SRNOMs; (d) Electrolyte concentrations at α=0.01 in the presence of pristine- and M_f-SRNOMs normalized to that in the absence of SRNOMs ($Q_{\alpha=0.01}$).

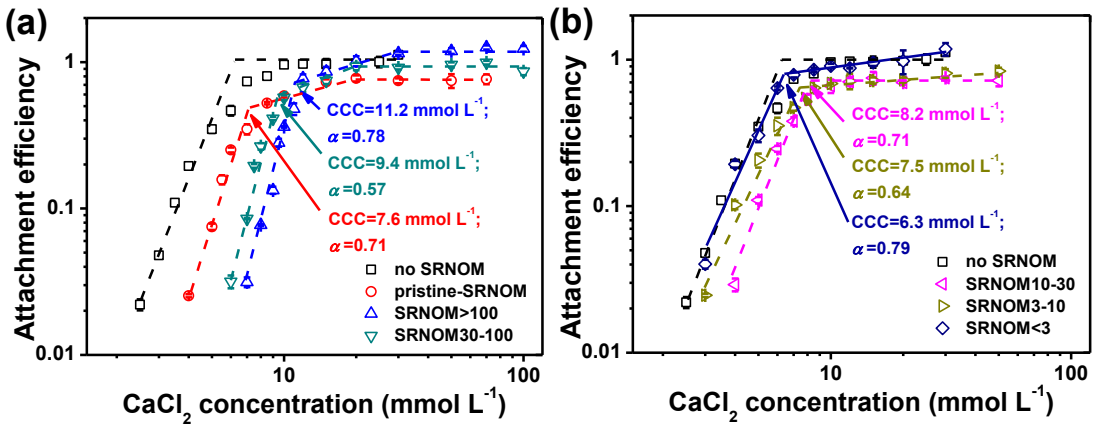

Figure 5. Attachment efficiency values of nC_{60} as a function of $CaCl_2$ concentration in the presence of pristine-SRNOM and M_f-SRNOMs. The symbol statements are the same as in Figure 4.

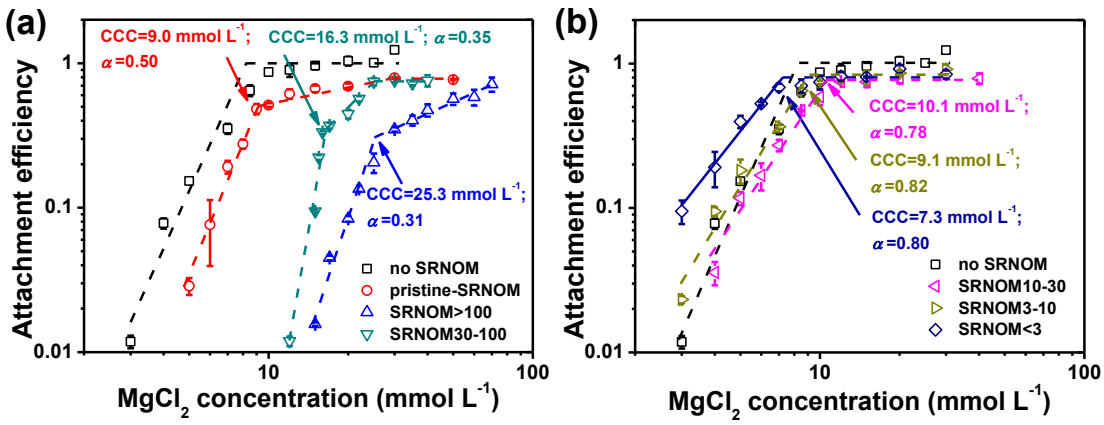

Figure 6. Attachment efficiency values of nC_{60} as a function of $MgCl_2$ concentration in the presence of pristine-SRNOM and M_f-SRNOMs. The symbol statements are the same as in Figure 4.

For TOC only:

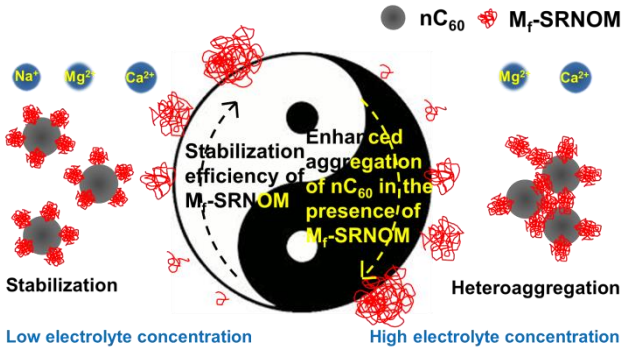
nC60
Mf-SRNOM
Na+
Mg2+
Ca2+
Mg2+
Ca2+
Stabilization efficiency of Mf-SRNOM
Enhanced aggregation of nC60 in the presence of Mf-SRNOM
Stabilization
Heteroaggregation
Low electrolyte concentration
High electrolyte concentration